Proceedings of the Jangjeon Mathematical Society
24 (2021), No. 4, pp. 543 - 554

www.jangjeon.or.kr
http://dx.doi.org/10.17777/pjms2021.24.4.543

Study of Photon Interaction and Photon Absorption Parameters for Bi-Sn-Zn Alloys

Vishali Rani†, Komalpreet Kaur, Yogesh K. Vermani*, Tejbir Singh

Department of Physics, Sri Guru Granth Sahib World University, Fatehgarh Sahib-140406, Punjab, INDIA

*Corresponding author's Email ID: yugs80@gmail.com
†Email ID: vishally25@gmail.com

Abstract. Lead is the toxic material which is conventionally used for shielding of highly penetrating and highly energetic gamma rays and X-rays. Due to high toxicity of lead metal, we aim to synthesize bismuth based alloy samples for possible radiation shielding application. Using the melt-quench technique, five bismuth containing alloy samples were synthesized with composition: $Bi_{50}Sn_{(50-x)}Zn_x$ $(x = 0, 10, 20, 30, 40)$. Mass attenuation coefficient (μ/ρ) values are compared with mass-energy absorption coefficient (μ_{en} /ρ) values in the energy region 1keV -20 MeV for the prepared alloy samples. Using photon attenuation coefficient and photon energy absorption coefficient values, we also estimated optimum thickness range for these Bi-Sn-Zn alloy compositions.

2010 Mathematics Subject Classification. 78A40; 81V10; 68U20
Key words: Gamma rays, radiation shielding properties, alloys.

INTRODUCTION

Due to astonishing properties of gamma rays, these radiations find applications in various fields such as space exploration, medicines, radiotherapy, food processing, atomic physics and many more. Apart from the numerous useful applications, gamma rays are also dangerous for healthy tissues and organs. Prolonged exposure to these radiations may lead to hazardous diseases such as skin irritation, nausea, tumor or even death. To reduce the intensity of these highly penetrating radiations, shielding is required. Radiation shielding materials should have high density (ρ) and high atomic number. Lead, concrete and mercury, for instance, are some of the traditional shielding materials. Beside pure metals, alloys are also preferred as these are mixture of metals or other elements (metals, non-metals, metalloids) which may enhance the radiation shielding properties of the material after mixing. Many researchers have investigated and explored different kinds of alloys, composites, glasses, polymers as gamma-ray shielding materials [1-6] in industries, radio-diagnosis, and medical appli-

Date of manuscript submission: November 15, 2019

cations. Kaur *et al.* [5] investigated the feasibility of Pb-Sn binary alloys as a gamma-ray shielding material. The effective atomic number Z_{eff} is found to increase with increase in concentration of element having high atomic number. Kaur *et al.* [6] investigated the feasibility of Pb-Zn alloys as gamma-ray shielding material with composition $Pb_xZn_{(100-x)}$ (with $x = 20, 40, 60, 80$). Some shielding parameters such as density (ρ), mass attenuation coefficient (μ_m), effective atomic number (Z_{eff}), electron density (N_e), half value layer (HVL), tenth value layer (TVL) were determined for these alloy compositions. These studies concluded that alloy with large weight fraction of element having higher atomic number may offer high effective atomic number and thus better shielding.

Another study regarding Bi-Pb based alloys was made by Shalaby [7]. Three fusible Bi-Pb based alloy systems namely Wood's alloy ($Bi_{50}Pb_{28}Sn_{12.5}Cd_{12.5}$), Newton's alloy ($Bi_{50}Pb_{31.2}Sn_{18.8}$), and Rose's alloy ($Bi_{50}Pb_{28}Sn_{22}$) were prepared by melt-spinning technique. A decrease in melting point was observed for Wood's alloy due to presence of cadmium. The Wood's alloy was also reported to show better radiation protection properties. These experimental observations revealed that one should systematically synthesize alloy systems with reduced or nil quantity of lead and investigate for their radiation shielding characteristics.

Nowadays, lead free compositions are in focus due to the toxicity of lead. Lead metal and its derivatives are known toxic carcinogens which are highly harmful for human health [8, 9, 10]. Therefore, radiation physicists have been continuously making efforts to develop materials for replacing lead and its derivatives as radiation shielding blocks [11, 12, 13, 14]. The aim of present study is to check the feasibility Bi-Sn-Zn alloys as gamma-ray shielding blocks on the basis of density measurement, estimation of mass attenuation coefficient (μ_m), mass-energy absorption coefficient (μ_{en}/ρ), and optimum thickness range (x).

MATERIALS AND METHODOLOGY

The melt-quenching technique has been adopted to prepare the samples of Bi-Sn-Zn alloys. The Bi, Sn and Zn metallic granules (with >99.9% purity procured from Loba Chemie Pvt. Ltd., Wodehouse Road, Mumbai, India) were weighed using digital balance (maximum capacity of 600 g and least count of 1 mg) in required amounts. The mixture is then heated in alumina crucible at 500°C for 30 minutes placed in an electric muffle furnace. The molten material is poured into cast iron mould (of dimensions 2×2×2 cm^3) at room temperature. The chemical composition and thickness of alloy samples prepared in the form of square shaped pellets are listed in

the table 1. The thickness of synthesized alloy samples lies between 0.564 and 0.800 cm for different wt. % compositions as shown in the table 1. The decrease in sample thickness with increase in Wt. % of Zn indicates that alloy sample gets more compact. The density of alloy samples has been calculated by Archimedes' principle by using the formula, $\rho = \frac{W_A}{W_A - W_B} \times 0.876$, where W_A is the weight of alloy sample in air and W_B is the weight of alloy sample in fluid (toluene with $\rho = 0.876\ g/cm^3$). Various radiation shielding parameters such as density, mass attenuation coefficient, mass–energy absorption coefficient, and optimum thickness range are measured for the prepared alloys.

To measure the mass attenuation coefficient of sample, we measure the transmitted beam intensity I through thickness `x' of alloys specimen as shielding material.

Alloy Sample	Elemental Composition (Wt. %)			Sample Thickness (cm)
	Bi	Sn	Zn	
$Bi_{50}Sn_{50}$ [S1]	50	50	0	0.800
$Bi_{50}Sn_{40}Zn_{10}$ [S2]	50	40	10	0.791
$Bi_{50}Sn_{30}Zn_{20}$ [S3]	50	30	20	0.724
$Bi_{50}Sn_{20}Zn_{30}$ [S4]	50	20	30	0.600
$Bi_{50}Sn_{10}Zn_{40}$ [S5]	50	10	40	0.564

TABLE 1. Chemical composition and thickness of prepared alloy samples.

The transmitted beam intensity I is related to incident beam intensity $I_\circ$ according to inverse exponential law:

$$I = I_\circ e^{-\mu x}, \tag{1}$$

$$\mu = \frac{1}{x} \ln\left(\frac{I_\circ}{I}\right). \tag{2}$$

Equation (2) is usually referred to as Lambert-Beer Law [1]. Here 'μ' rep-

resents the linear attenuation coefficient. Mass attenuation coefficient is then evaluated as [3]:

$$\mu_m = \frac{\ln\left(I_\circ / I\right)}{\rho \cdot x}, \tag{3}$$

where, ρ is the density of the shielding material (in g/cm^3). We also compute the mass attenuation coefficient values for these alloys specimens using WinXCom database [15]. These values have been computed using a mixture rule [16]:

$$\mu_m = \sum_i \omega_i \left(\mu_m\right)_i , \tag{4}$$

where $(\mu_m)_i$ is the mass attenuation coefficient for individual elements in the mixture and ω_i is the weight fraction of the i^{th} element in the mixture. We also compute the mass-energy absorption coefficient for the alloy samples synthesized. The mass-energy absorption coefficient (μ_{en}/ρ) has been computed using the formula [17]:

$$(\mu_{en} / \rho)_{alloy} = \sum_i \ \omega_i \cdot (\mu_{en}/\rho)_i, \tag{5}$$

where $(\mu_{en}/\rho)_i$ is the mass-energy absorption coefficient of i^{th} constituent element present in the alloy sample. The μ_{en}/ρ values of respective constituent elements have been taken from standard database of NIST [18]. The mass-energy absorption coefficient takes into account the fraction of total incident photon energy transferred to kinetic energy of charged particles during photon interaction with the material. One may note that this component also takes into account energy carried by bremsstrahlung and other escaping secondary particles. The mass-energy absorption coefficient plays an important role in estimation of exposure and absorbed dose in medical radiation physics [18, 19].

RESULTS AND DISCUSSION

Density of different bismuth based alloys samples is measured with values as indicated in table 2. From precursory computations as shown in the table 2, it can be seen that the density ρ of an alloy sample increases with increase in weight fraction of Zn metal (and decrease in the weight fraction of Sn metal). Using WinXCom software, mass attenuation coefficient values are also calculated for different alloy samples. Variation in the alloys' elemental composition is observed to hardly effect the mass attenuation coefficient values. This is largely due to the fact that in the Compton scattering region, as per the assumption of free electron requirement, there is least dependence on the Z_{eff}. As far as photon energy dependence of μ_m is concerned, the μ_m varies inversely with photon energy as clear from the tabular values indicated at gamma-ray source energies 511, 662, and 1250

keV. The photon energy values chosen correspond to the energies of gamma –ray sources available for experimental measurement of mass attenuation coefficient values.

In Fig. 1, we compare mass-energy absorption coefficient (μ_{en}/ρ) values with mass attenuation coefficient (μ_m) values for the alloy samples S1, S2, S3, S4, and S5 respectively. Also shown in the Fig. 1 are the mass attenuation coefficient values $(\mu_m)_{exp}$ obtained experimentally for the prepared alloy samples at photon energies of 511, 662 and 1250 keV, respectively. The inverse energy dependence of mass attenuation coefficient values is due to the fact that photoelectric absorption cross section varies inversely with incident energy as $\sigma_{PP} \propto 1/E^{3.5}$. It can be seen that mass attenuation coefficient values obtained experimentally are in good agreement with those computed using WinXCom software database [15] in the Compton scattering region. Shaded region in the Fig. 1 represents Compton scattering regime, where increase in photon energy is observed to have negligible influence on mass attenuation coefficient (μ_m) and mass-energy absorption coefficient (μ_{en}/ρ) values. The variation of mass-energy absorption coefficient with photon energy follows the same trend as followed by mass attenuation coefficient values $\mu_m(=\mu/\rho)$. Initial μ_m and μ_{en}/ρ values are maximal at lower end of photon energy spectrum. The fall in μ_m (or, μ_{en}/ρ) values with increase in photon energy happens due to inverse energy dependence of cross-section for photoelectric absorption ($\sim 1/E^{3.5}$) as discussed above. In photoelectric absorption domain, there is complete absorption of photon energy into the interacting material, hence $\mu_m(=\mu/\rho)$. Initial μ_m and μ_{en}/ρ values almost coincide in this region. With further increase in energy, contribution from Compton scattering cross-section results into marked difference in μ_m and μ_{en}/ρ values as clear from the Fig. 1. This happens due to the fact that incident photon transfers only partial energy to the interacting material resulting into μ_{en}/ρ values lower than the μ_m values. These values attain a minimum around 2 MeV. This trend is found to be uniform across all the alloy specimens studied here. In the photon energy range 0.8 MeV to 3 MeV, there is very little variation in the values of photon attenuation and photon energy absorption coefficients. Beyond 3 MeV, pair production appears to be dominant process. In this high energy regime, there is observed a small increment again in the mass attenuation coefficient and mass-energy absorption coefficient values with photon energy. The optimum thickness range is obtained from the product of linear attenuation coefficient μ and

Alloy Sample	Photon Energy (keV)	Density (g/cm^3)	μ_m (cm^2/g)	μ (cm^{-1})	Optimum Thickness Range (cm)
$Bi_{50}Sn_{50}Zn_{00}$	511	8.626	0.1261	1.0879	0.4596 - 0.6434
	662	8.626	0.0940	0.8112	0.6163 - 0.8628
	1250	8.626	0.0552	0.4764	1.0493 - 1.4691
$Bi_{50}Sn_{40}Zn_{10}$	511	8.649	0.1252	1.0835	0.4615 - 0.6460
	662	8.649	0.0938	0.8113	0.6162 - 0.8627
	1250	8.649	0.0554	0.4795	1.0428 - 1.4599
$Bi_{50}Sn_{30}Zn_{20}$	511	8.683	0.1244	1.0804	0.4628 - 0.6479
	662	8.683	0.0935	0.8125	0.6154 - 0.8615
	1250	8.683	0.0556	0.4831	1.0349 - 1.4489
$Bi_{50}Sn_{20}Zn_{30}$	511	8.887	0.1235	1.0982	0.4553 - 0.6374
	662	8.887	0.0933	0.8295	0.6028 - 0.8439
	1250	8.887	0.0558	0.4962	1.0075 - 1.4105
$Bi_{50}Sn_{10}Zn_{40}$	511	8.971	0.1227	1.1010	0.4541 - 0.6358
	662	8.971	0.09310	0.8352	0.5986 - 0.8381
	1250	8.971	0.0560	0.5027	0.9945 - 1.3923

TABLE 2. The density, mass attenuation coefficient, linear attenuation coefficient and optimum thickness range of prepared alloy samples measured at gamma–ray energies of 511 keV, 662 keV, and 1250 keV, respectively.

thickness `$x'$ of the alloy sample, provided the product `$\mu x'$ should lie in the range $0.5 \leq \mu x \leq 0.7$. This optimum thickness results in accurate measurement of mass attenuation coefficient values [20]. As illustrated in the table 2, the optimum thickness range is observed to increase with the incident photon energy. In other words, the optimum thickness range increases with decrease in linear attenuation coefficient μ. We also estimated the optimum thickness range using photon energy absorption coefficient μ_{en}/ρ values. The minimum (and, maximum) values of optimum thickness range *i.e.* x_{min} (and, x_{max}) obtained using the condition $0.5 \leq \mu_{en} \cdot x \leq 0.7$ are computed for the alloy samples S1, S2, S3, S4, and S5, respectively. These values computed as function of photon energy are displayed in Fig. 2. Upper panel of Fig. 2 gives variation of optimum thickness range with photon energy in the photoelectric absorption regime. For all the alloy compositions studied in this paper, the optimum thickness range (*i.e.* x_{min} and x_{max} values) increases with incident photon energy. In this low photon energy regime, optimum thickness range is found to vary rapidly with photon energy due to strong energy dependence of photoelectric absorption cross-section ($\sim 1/E^{3.5}$) [21]. For the alloy samples prepared, optimum thickness range varies from $10^{-5}cm$ to $10^{-1}cm$. It implies that an alloy sample prepared for measuring the mass attenuation coefficient at a particular energy can't be employed at another photon energy in photoelectric absorption regime. In such a low energy regime, very thin samples of the order of few microns are required to attain effective gamma-ray attenuation.

As shown in the lower panel of Fig. 2, beyond photoelectric absorption region, the optimum thickness range varies from $0.5\ cm$ to $4\ cm$. Above 200 keV, the optimum thickness range keeps increasing with photon energy and gets saturated around 2 MeV, where contribution due to pair production process initiates. This suggests that alloy sample of given thickness can be easily employed for measurement of the mass attenuation coefficient over wide photon energy region. For instance, alloy sample of thickness $2.5\ cm$ can be used for measuring μ_m values over wide energy range from 1 MeV to 20 MeV spanning Compton scattering and pair-production domains.

As far as lead containing alloys are concerned, Kaur *et al.* [20] investigated the shielding properties of binary Pb-Sn alloys. $Pb_{60}Sn_{40}$ alloy composition was found to have optimum thickness range 0.647-0.905 cm at 662 keV and density equal to 8.055 g/cm^3. In the present case, for lead free binary alloy composition $Bi_{50}Sn_{50}$, the optimum thickness range is 0.6163-0.8628 cm at 662 keV photon energy. The optimum thickness range for $Bi_{50}Sn_{50}$ is still smaller than that of binary alloy $Pb_{60}Sn_{40}$ at 662 keV. At

511 keV also, similar trend has been observed for optimum thickness range. The density of $Bi_{50}Sn_{50}$ alloy sample is measured to be 8.626 g/cm^3 which is also higher than density of $Pb_{60}Sn_{40}$ alloy sample. Moreover, the mass attenuation coefficient value of 0.094 cm^2/g for $Bi_{50}Sn_{50}$ is comparable with value of 0.096 cm^2/g obtained in case of $Pb_{60}Sn_{40}$ alloy with higher wt% of Pb.

In view of lead's toxicity and human poisoning [22], bismuth based alloy compositions are better substitute as gamma rays shielding blocks. Moreover, bismuth based alloy compositions are environmentally friendly for their safe disposal and recycling.

CONCLUSIVE REMARKS

In the present work, we have investigated photon-interaction and photon-energy absorption parameters for effectiveness of Bi-Sn-Zn alloys as gamma-rays shielding material. We measured the density, optimum thickness range, mass attenuation coefficient and mass-energy absorption coefficient for the alloy samples synthesized. The density of Bi-Sn-Zn alloy samples is observed to increase, however, marginally with increase in weight fraction of Zn metal. Like density, the mass attenuation coefficient values are also hardly affected by increase in the weight fraction of Zn element in the alloy sample. Using the measured density, mass attenuation coefficient values were determined experimentally which are in close agreement with those computed using WinXCom software database.

From the photon attenuation coefficient and photon energy absorption coefficient values, we also estimated optimum thickness range for the prepared alloy samples over wide range of photon energies. The optimum thickness range of these alloy specimens is found to increase with increase in photon energy, the trend which is just opposite to that of mass attenuation coefficient and mass–energy absorption coefficient. In photoelectric absorption energy regime, optimum thickness range is much narrower of the order of few microns. In Compton and pair production energy regime, on the other hand, the optimum thickness range is quite wider (of the order of few centimeters). It, therefore, becomes easier to handle and work with alloy samples of larger thickness in Compton and pair production energy regime.

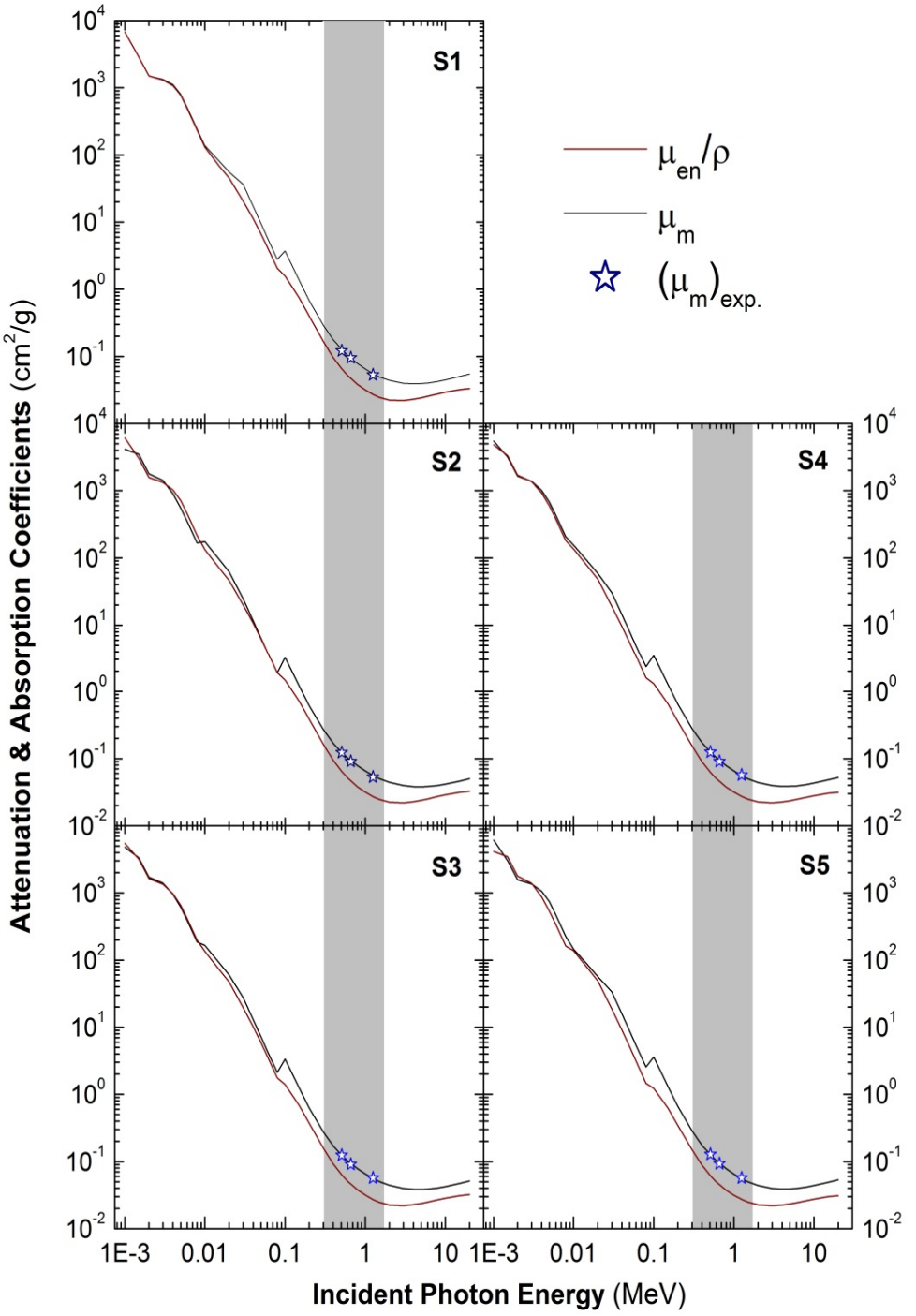

Figure 1. Variation of photon attenuation coefficient ($\boldsymbol{\mu_m}$) and photon absorption coefficient ($\boldsymbol{\mu_{en}/\rho}$) as a function of incident photon energy for selected Bi-Sn-Zn alloy specimens. Experimentally determined mass attenuation coefficient $(\boldsymbol{\mu_m})_{exp}$ values are shown by asterisk symbols at photon energies of 511, 662, and 1250 keV, respectively.

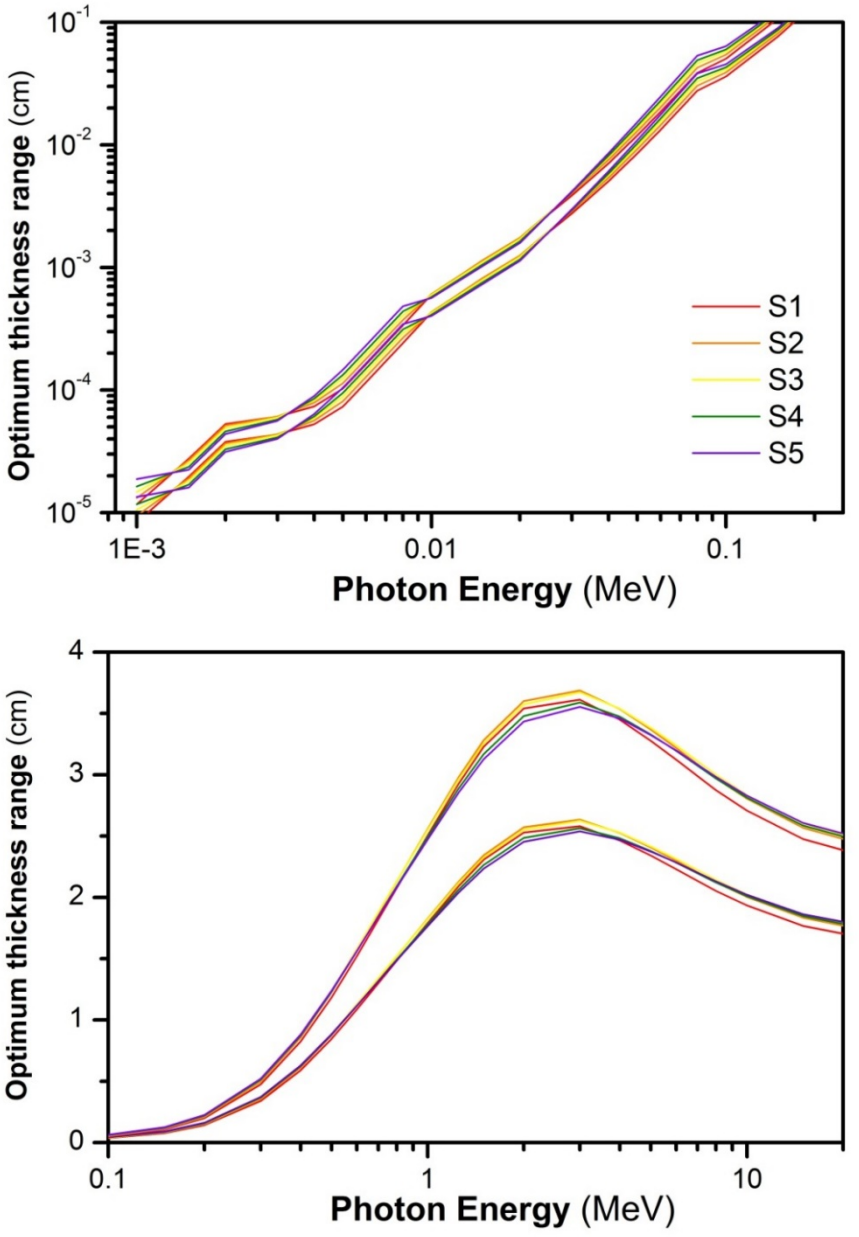

Figure 2. Variation of optimum thickness range in the photoelectric absorption energy region (top panel) and Compton and pair production energy domains (bottom panel) as a function of incident photon energy for selected Bi-Sn-Zn alloy samples.

References

[1] H. Singh, J. Sharma, and T. Singh, *Nucl. Eng. Technol.* **50** (2018), 1364-1371.

[2] M. I. Sayyed, Shams A. M. Issa, H. O. Tekin, and Yasser B. Saddeek, *Mater. Chem. Phys.* **217** (2018), 11-22

[3] T. Singh, A. Kaur, J. Sharma, and P. S. Singh, *Int. J. Eng. Sci. Technol.* **21** (2018), 1078-1085.

[4] M. Kamal, M. El-Tonsy, Abu B. El-Bediwi, and E. Kashita, *Phys. Stat. Sol(a)*. **201** (2004), 2029–2034.

[5] S. Kaur, A. Kaur, P. S. Singh, and T. Singh, *Prog. Nucl. Energ.* **93** (2016), 277-286.

[6] T. Kaur, J. Sharma, and T. Singh, *Int. J. Pure Appl. Phys.* **13** (2017), 222-225.

[7] R. M. Shalaby, *J. Mater. Sci. Technol*. **25** (2009), 449-453.

[8] A. Demayo, M. C. Taylor, K. W. Taylor, P. V. Hodson, and P. B. Hammond; Toxic effects of lead and lead compounds on human health, aquatic life, wild life plants, and livestock, *C R C Critical Re views in Environmental Control*, Vol. **12 (4)** (1982), 257-305, Taylor & Francis.

[9] V. Mudgal, N. Madaan, A. Mudgal, R. B. Singh, and S. Mishra, *Open Nutraceuticals J*. **3** (2010), 94-99.

[10] A. L. Wani, A. Ara, and J. A. Usmani, *Interdiscip. Toxicol*. **8(2)** (2015), 55-64.

[11] J. Kaewkhao, J. Laopaiboon, and W. Chewpraditkul, *J. Quant. Spe trosc. Radiat. Transfer* **109 (7)** (2008), 1260-1265.

[12] I. Han, M. Aygun, L. Demir, and Y. Sahin, *Ann. Nucl. Energy* **39** (2012), 56-61.

[13] F. Akman, M. I. Sayyed, M. R. Kaçal, and H. O. Tekin, *J. Alloys Compd.* **772** (2019), 516-524.

[14] F. Akman, M. R. Kaçal, M. I. Sayyed, and H. A. Karataş, *J. Alloys Compd.* **782** (2019), 315-322.

[15] L. Gerward, N. Guibert, K. B. Jensen, and H. Leving, *Radiat. Phys. Chem*. **71**, 653-654 (2004); M. J. Berger and J. H. Hubbell "XCOM:

Photon Cross Sections Database", Web version 1.2 (1999), Available at *http://physics.nist.gov/xcom.*

[16] R. S. Niranjan, B. Rudraswamy, and N. Dhananjaya, *Pramana J. Phys.* **78** (2012), 451- 458.

[17] S. R. Manohara, S. M. Hanagodimath, and L. Gerward, *Phys. Med. Biol*. **53(20)** (2008), 377-386.

[18] J. H. Hubbell and S. M. Seltzer, NISTIR 5632, 1995.

[19] J. H. Hubbell, *J. Appl. Radiat. Isot*. **33** (1982), 1269-1290.

[20] T. Kaur, J. Sharma, and T. Singh, *Nucl. Eng. Technol*. **3** (2017), 1–5.

[21] T. Singh, Rajni, U. Kaur, and P. S. Singh, *Ann. Nucl. Energy* **37** (2010), 422 - 427.

[22] P. B. Tchounwou, C. G. Yedjou, A. K. Patlolla, and D. J. Sutton, *Exp. Suppl.* **101** (2012), 133–164.